Supporting Information for

Fluorination switches CO–arene binding to a π-hole regime, enabling nonclassical carbonyl behaviour

Imanol Usabiaga, Weixing Li, Camilla Calabrese, Ahmet Altun, Assimo Maris, Sonia Melandri, Giovanni Bistoni,* Luca Evangelisti*

***Corresponding Authors:** giovanni.bistoni@unipg.it; luca.evangelisti6@unibo.it

Contents

S1. Spectral and Thermodynamic Parameters

S1.1. Experimental Details

The molecular complexes have been generated in a supersonic expansion under optimized conditions. A gas mixture of about 1% of CO (commercial sample used without any further purification) in helium of about 0.3 MPa was passed over C_6F_6 (commercial sample used without any further purification) at 273 K. All the details of the COBRA-type FTMW spectrometer operating in the 6 - 18 GHz range have been described previously. In brief, the gas mixture is expanded through a solenoid valve (the Series 9 - General Valve) into the Fabry-Perot cavity (10^{-5} Pa). The spectral line positions were determined after Fourier transformation of the time domain signal with 8k data points, recorded with 100 ns sample intervals. Due to the Doppler Effect, each transition appears as a doublet. The line position is calculated as the arithmetic mean of the frequencies of the Doppler components. The estimated accuracy of the frequency measurements is better than 1 kHz and the line separated by more than 5 kHz are resolvable.

S1.2. Computational Details

Conformational search was performed by using the AMBER[1] force field implemented in Schrödinger Suite Macromodel[2] software as well as at the B3LYP-D3(BJ)[3] level with the def2-TZVP[4] basis set by using ORCA[5] program package based on version 5.0. For SCF convergence and geometry optimizations very tight criteria of ORCA were used. Unless stated otherwise, spectroscopic and thermodynamic calculations were performed at the B3LYP-D3(BJ)/def2-TZVP geometries with the ORCA program package. For more accurate estimations of ΔG values, RRHO approach of Grimme[6] that treats modes with frequencies below 35 cm^{-1} as free rotors instead of harmonic vibrations was used. Harmonic approximation results in noticeably larger ΔG values.

S1.3. Results for $C_6F_6\cdots CO$

Table S1. Spectroscopic parameters and relative conformational energies of $C_6F_6\cdots CO$ calculated at the B3LYP-D3(BJ)/def2-TZVP level

	C6F6_CO_01	C6F6_CO_02
A (MHz)	582	630
B (MHz)	582	622
C (MHz)	515	509
μ_a (D)	0.0	-0.04
μ_b (D)	0.0	0.0
μ_c (D)	-0.22	-0.06
ΔE (kJ/mol)	0	2.0
ΔG_{0K} (kJ/mol)	0	1.6
ΔG_{298K} (kJ/mol)	0	-0.5

Table S2. Binding energy ΔE (kJ/mol) calculated in gas phase at the B3LYP-D3(BJ)/def2-TZVP and DLPNO-CCSD(T)/CBS(3/4) levels using the B3LYP-D3(BJ)/def2-TZVP geometries with thermochemical corrections included at the B3LYP-D3(BJ)/def2-TZVP level.

	B3LYP-D3(BJ)/def2-TZVP				DLPNO-CCSD(T)/CBS(3/4)			
	ΔG_{298K}	ΔH	$\Delta G_{0K} = -D_0$	$\Delta E = -D_e$	ΔG_{298K}	ΔH	$\Delta G_{0K} = -D_{00}$	$\Delta E = -D_e$
C6F6_CO_01	30.5	-7.2	**-7.3**	-8.6	32.2	-5.5	**-5.6**	-6.9
C6F6_CO_02	31.5	-5.3	**-5.6**	-6.6	33.1	-3.8	**-4.1**	-5.1

Table S3. Experimental transition frequencies of $C_6F_6\cdots CO$: Assignments, measured transition frequencies (ν in MHz), and deviation between experimental and calculated[a] frequencies (Δν in MHz)

J'	*K'*	*J*	*K*	ν	Δν
6	0	5	0	6898.1998	0.0012
6	1	5	1	6898.1738	0.0001
6	2	5	2	6898.0984	-0.0005
6	3	5	3	6897.9751	0.0007
6	4	5	4	6897.8003	0.0003
6	5	5	5	6897.5770	0.0011
7	0	6	0	8047.8357	-0.0009
7	1	6	1	8047.8073	-0.0002
7	2	6	2	8047.7191	-0.0012
7	3	6	3	8047.5750	0.0000
7	4	6	4	8047.3715	-0.0001
7	5	6	5	8047.1093	-0.0007
7	6	6	6	8046.7895	-0.0009
8	0	7	0	9197.4461	0.0000
8	1	7	1	9197.4136	0.0006
8	2	7	2	9197.3125	-0.0008
8	3	7	3	9197.1474	0.0001
8	4	7	4	9196.9148	0.0000
8	5	7	5	9196.6154	-0.0004

Table S3. Continued

J'	*K'*	*J*	*K*	ν	Δν
8	6	7	6	9196.2509	0.0003
8	7	7	7	9195.8186	-0.0001
9	0	8	0	10347.0252	0.0020
9	1	8	1	10346.9854	-0.0004
9	2	8	2	10346.8743	0.0005
9	3	8	3	10346.6871	0.0001
9	4	8	4	10346.4230	-0.0023
9	5	8	5	10346.0914	0.0023
9	6	8	6	10345.6785	0.0004
9	7	8	7	10345.1932	0.0008
9	8	8	8	10344.6301	-0.0017
10	0	9	0	11496.5635	0.0000
10	1	9	1	11496.5207	-0.0013
10	2	9	2	11496.3981	0.0005
10	3	9	3	11496.1908	0.0008
10	4	9	4	11495.9000	0.0006
10	5	9	5	11495.5279	0.0022
10	6	9	6	11495.0688	-0.0002
10	7	9	7	11494.5284	-0.0009
10	8	9	8	11493.9059	-0.0006
10	9	9	9	11493.1980	-0.0028
11	0	10	0	12646.0610	-0.0022
11	1	10	1	12646.0177	0.0000
11	2	10	2	12645.8800	-0.0006
11	3	10	3	12645.6527	0.0004
11	4	10	4	12645.3322	-0.0004
11	5	10	5	12644.9218	0.0001
11	6	10	6	12644.4185	-0.0007
11	7	10	7	12643.8264	0.0007
11	8	10	8	12643.1378	-0.0028
11	9	10	9	12642.3673	0.0030
11	10	10	10	12641.4968	0.0002
12	0	11	0	13795.5197	0.0014
12	1	11	1	13795.4693	0.0008
12	2	11	2	13795.3186	-0.0003
12	3	11	3	13795.0718	0.0019
12	4	11	4	13794.7210	-0.0001
12	5	11	5	13794.2701	-0.0026
12	6	11	6	13793.7251	0.0003
12	7	11	7	13793.0812	0.0040
12	8	11	8	13792.3299	0.0000
12	9	11	9	13791.4830	0.0000
13	1	12	1	14944.8702	-0.0002
14	0	13	0	16094.2743	-0.0033
14	1	13	1	16094.2211	0.0016

S1.5. Results for $C_6H_6\cdots CO$

Table S4. Spectroscopic parameters and relative conformational energies of $C_6H_6\cdots CO$ calculated at the B3LYP-D3(BJ)/def2-TZVP level

	$C_6H_6\cdots CO$
A (MHz)	2731
B (MHz)	1594
C (MHz)	1551
μ_a (D)	0.2
μ_b (D)	-0.1
μ_c (D)	0.0

S2. Dipole Moment and Partial Charges of CO

Table S5. Dipole moment (μ in D) and Mulliken partial charges (Q in e) of CO at HF/ aug-cc-pVQZ and B3LYP-D3(BJ)/def2-TZVP levels

Method	μ	Q_C	Q_O
HF	0.250	0.35	-0.35
B3LYP-D3(BJ)	-0.108	-0.11	0.11

B3LYP-D3(BJ) predicts the experimentally[9] determined dipole moment (–0.12 D) and the partial charges (negative on C; positive on O) correctly, which are also consistent with the results of large CI calculations.[10] In contrast, HF predicts dipole moment and partial charges not only in sign reversed but also in magnitude quite larger.

S3. Molecular Electrostatic Potentials at the B3LYP-D3(BJ)/def2-TZVP Level

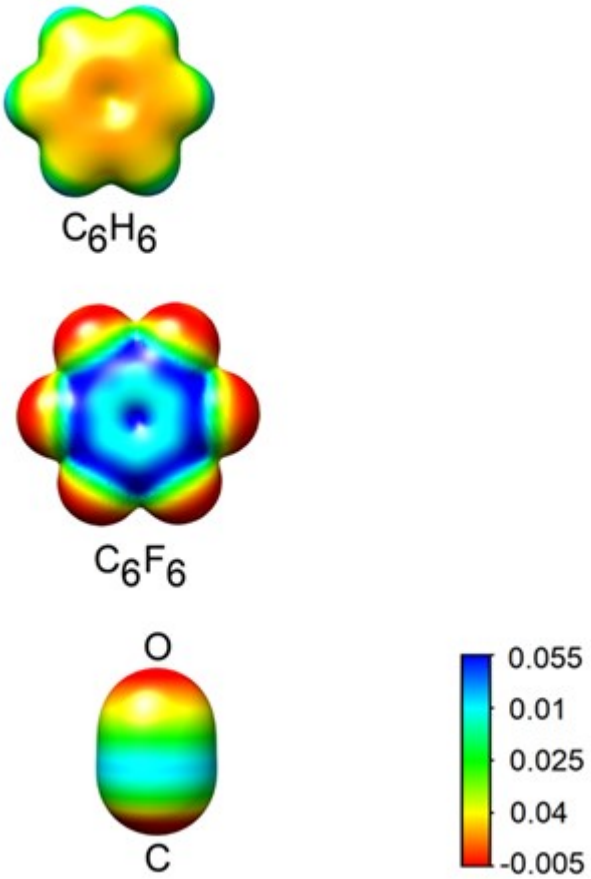

Figure S1. Molecular electrostatic potential of isolated ligands mapped onto the corresponding electron density (isosurface contour value: ±0.004 e·bohr^{-3}) at the B3LYP/def2-TZVP level. The color bar is given between –0.005 E_h/e (red) and +0.055 E_h/e (blue).

S4. Relative DLPNO-CCSD(T)/LED Energies

All the calculations were performed at the B3LYP-D3(BJ)/def2-TZVP geometries described in section S1.2. Relative energies were calculated as the difference in the binding energies (ΔE) and free energies (ΔG) of the adducts. Analogously, decomposed contributions like dispersion and non-dispersion to the relative energies were calculated as the difference in the corresponding energies of the adducts.

In DLPNO-CCSD(T) calculations,[11] SCF references were obtained within the RIJK approach.[12] TightPNO settings were used. All electron pairs were included in the coupled treatment. The augmented Hessian Foster-Boys scheme[13] was employed for localizing occupied orbitals. The aug-cc-pVnZ (n = T and Q) and their matching standard auxiliary basis sets were used.[14] The results were extrapolated to the complete basis set (CBS) limit as described previously.[15] Interaction energies were corrected for basis set superposition error (BSSE).[16] Geometrical preparation

contribution to the binding energy is zero for all adducts. Therefore, binding energy (ΔE) and interaction energy (ΔE_{int}) contributions to the relative energies are the same for these cases. Vibrational and entropic contributions computed at the B3LYP-D3(BJ)/def2-TZVP level were added to the DLPNO-CCSD(T) energetics to obtain ΔG_{0K} and ΔG_{298K}.

The BSSE-corrected DLPNO-CCSD(T)/CBS interaction energies were decomposed into dispersive and non-dispersive contributions by using Local Energy Decomposition (LED)[17] scheme. The (T) contribution to the dispersion energy was computed as described in ref. 18. LED was performed by localizing virtual orbitals (PNOs) using the Foster-Boys scheme.[13]

HF/CBS, DLPNO-CCSD(T)/CBS, and B3LYP-D3(BJ)/def2-TZVP relative energies are compared in Table S5 for the fluorinated adducts, respectively. Dispersion and non-dispersion contributions to the relative DLPNO-CCSD(T)/CBS interaction energies obtained by using the LED scheme are also provided in Tables S6. From this table, it is clear that proper treatment of dynamic electron correlation is extremely important. While B3LYP-D3(B3) provides reasonably close energetics to DLPNO-CCSD(T) reference, MP2 overestimates relative energies noticeably, consistent with previous findings on analogous aromatic structures.[19]

Table S6. Relative energies (kJ/mol) calculated in gas phase at the B3LYP-D3(BJ)/def2-TZVP and DLPNO-CCSD(T)/CBS levels for the fluorinated adducts together with decomposed dispersion and non-dispersion contributions to DLPNO-CCSD(T)/CBS energetics obtained by using the LED scheme

Adducts	HF	B3LYP -D3(BJ)			DLPNO-CCSD(T)			LED of ΔE_{int}	
	ΔE	ΔG_{298K}	ΔG_{0K}	ΔE	ΔG_{298K}	ΔG_{0K}	ΔE	ΔE_{disp}	$\Delta E_{no\text{-}disp}$
Perpendicular C-coordinated									
C6F6_CO_01	0	0	0	0	0	0	0	0	0
Perpendicular O-coordinated									
C6F6_CO_02	-2.2	-0.5	1.6	2.0	-0.5	1.5	1.9[a]	0.8	1.1

[a] The corresponding MP2/CBS value is 3.0 kcal/mol. Therefore, MP2 overestimates relative energies for the current systems.

S5. DID Plots at the DLPNO-CCSD/LED Level

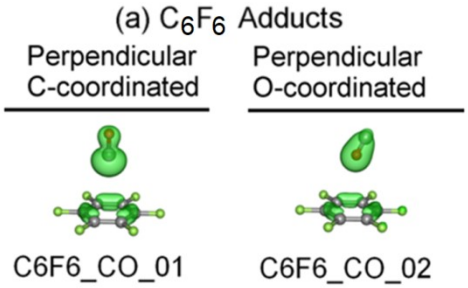

Figure S2. DLPNO-CCSD/LED dispersion interaction density (DID)[17(b)] plots of fluorinated adducts (isosurface contour value: 0.01 kcal/mol·bohr^{-3})

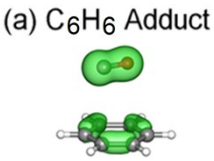

Figure S3. DLPNO-CCSD/LED dispersion interaction density (DID)[17(b)] plots of non-fluorinated adduct (isosurface contour value: 0.01 kcal/mol·bohr^{-3})

S6. Decomposition of B3LYP-D3(BJ)/def2-TZVP Relative Energies and Electron Density Deformation Plots

B3LYP-D3(BJ)/def2-TZVP relative energies were decomposed into frozen state (ΔE_0), orbital relaxation ($\Delta E_{o.r.}$), and dispersion (ΔE_{disp}) contributions (see Table S7), as described in ref. 17(b). ΔE_0 is the difference in the energies associated to the antisymetrized product of the wave functions of the noninteracting fragments at different adduct geometries. $\Delta E_{o.r.}$ corresponds to the difference in the energies associated with the charge transfer and polarization effects upon adduct formation for different adducts. ΔE_{disp} is the difference in the D3(BJ) contribitions of the adducts. Note that ΔE_{disp} values of B3LYP-D3(BJ)/def2-TZVP (see Table S6) and DLPNO-CCSD(T)/LED (see Table 6) are reasonably close to each other. One-electron density deformations upon orbital relaxations (see ref. 17(b)) are shown for fluorionated and non-fluorionated adducts in Figures S4 and S5.

Table S7. Decomposition of the gas-phase B3LYP-D3(BJ)/def2-TZVP relative energies (ΔE in kJ/mol) for the fluorinated adducts

	ΔE	ΔE_0	$\Delta E_{o.r.}$	ΔE_{disp}
Perpendicular C-coordinated				
C6F6_CO_01	0	0	0	0
Perpendicular O-coordinated				
C6F6_CO_02	2.0	-1.3	1.6	1.6

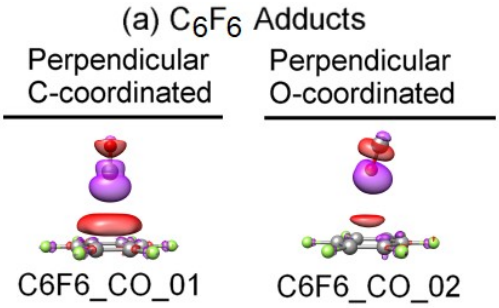

Figure S4. B3LYP/def2-TZVP one-electron density deformation upon fluorinated adduct formation (isosurface contour value: ±0.0002 e·bohr^{-3})

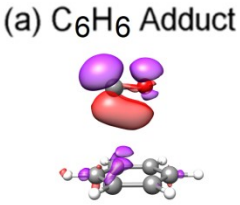

Figure S5. B3LYP/def2-TZVP one-electron density deformation upon non-fluorinated adduct formation (isosurface contour value: ±0.0002 e·bohr^{-3})

S7. Optimized Cartesian Coordinates (Å) at the B3LYP-D3(BJ)/def2-TZVP Level

C_6H_6

	x	y	z
C	1.339662	0.363153	0.508920
C	0.354476	1.344502	0.503762
C	-0.988402	0.981986	0.497942
C	-1.345634	-0.362318	0.497253
C	-0.360447	-1.343665	0.502412
C	0.982430	-0.981151	0.508231
H	2.385009	0.645747	0.513511
H	0.632958	2.390954	0.504309
H	-1.755710	1.746272	0.493882
H	-2.390965	-0.644908	0.492663
H	-0.638934	-2.390134	0.501865
H	1.749728	-1.745425	0.512291

C_6F_6

	x	y	z
C	1.337488	0.362426	0.508935
C	0.353753	1.342321	0.503768
C	-0.986720	0.980302	0.497928
C	-1.343473	-0.361593	0.497242
C	-0.359720	-1.341473	0.502409
C	0.980757	-0.979476	0.508250
F	2.623043	0.709601	0.514545
F	0.695855	2.629239	0.504415
F	-1.930150	1.920062	0.492983
F	-2.629018	-0.708767	0.491625
F	-0.701829	-2.628399	0.501755
F	1.924182	-1.919227	0.513187

$C_6H_6\cdots CO$

	x	y	z
C	-0.533945	1.506524	0.000000
C	-0.679260	0.826562	-1.204400
C	-0.966394	-0.533988	-1.204532
C	-1.108323	-1.214871	0.000000
C	-0.966394	-0.533988	1.204532
C	-0.679260	0.826562	1.204400
H	-0.305589	2.564872	0.000000
H	-0.564786	1.355930	-2.142006
H	-1.075358	-1.064730	-2.142009
H	-1.324894	-2.275567	0.000000
H	-1.075358	-1.064730	2.142009
H	-0.564786	1.355930	2.142006
C	2.275731	-1.178088	0.000000
O	2.555052	-0.087882	0.000000

$C_6F_6\cdots CO\_1$

	x	y	z
C	1.336589	0.362358	0.520707
C	0.353415	1.341660	0.515955
C	-0.986301	0.979901	0.510178
C	-1.342789	-0.361232	0.509254
C	-0.359647	-1.340569	0.514025
C	0.980073	-0.978789	0.519749
F	2.622691	0.709696	0.518739
F	0.695740	2.629095	0.509313
F	-1.930072	1.919995	0.497645
F	-2.628823	-0.708589	0.496092

$C_6F_6\cdots CO\_2$

	x	y	z
C	1.078444	0.653838	0.668127
C	-0.082007	1.386305	0.460224
C	-1.287220	0.731398	0.247891
C	-1.331842	-0.655899	0.243477
C	-0.171323	-1.388334	0.451522
C	1.033838	-0.733370	0.663723
F	2.236679	1.282188	0.863882
F	-0.037804	2.717554	0.458301
F	-2.400039	1.434052	0.043614
F	-2.487585	-1.284280	0.035716

F	-0.701893	-2.628006	0.505593	F	-0.213112	-2.719603	0.442145
F	1.923936	-1.918907	0.516933	F	2.149162	-1.436042	0.855881
C	0.011992	-0.000175	-2.739303	C	1.204443	0.013706	-3.528658
O	0.026741	-0.006166	-3.863540	O	0.561287	-0.000401	-2.604939

CO

	x	y	z
C	0.011363	0.000588	-2.690370
O	0.026118	-0.005329	-3.815334

S8. References

(1) Weiner, S. J.; Kollman, P. A.; Nguyen, D. T.; Case, D. A., All-atom AMBER, *J. Comput. Chem.* **1986**, *7*, 130.

(2) Mohamadi, F.; Richards, N. G. J.; Guida, W. C.; Liskamp, R.; Lipton, M.; Caufield, C.; Chang, G.; Hendrickson, T.; Still, W. C., Macromodel-An Integrated Software System for Modeling Organic and Bioorganic Molecules Using Molecular Mechanics, *J. Comput. Chem.* **1990**, *11*, 440.

(3) **(a)** Becke, A. D. Density-Functional Thermochemistry. III. The Role of Exact Exchange. *J. Chem. Phys.* **1993**, *98*, 5648−5652. **(b)** Lee, C.; Yang, W.; Parr, R. G. Development of the Colle-Salvetti Correlation-Energy Formula into a Functional of the Electron Density. *Phys. Rev. B* **1988**, *37*, 785−789. **(c)** Becke, A. D. Density-Functional Exchange-Energy Approximation with Correct Asymptotic Behavior. *Phys. Rev. A* **1988**, *38*, 3098−3100. **(d)** Grimme, S.; Ehrlich, S.; Goerigk, L. Effect of the Damping Function in Dispersion Corrected Density Functional Theory. *J. Comput. Chem.* **2011**, *32*, 1456−1465.

(4) **(a)** Weigend, F. Accurate Coulomb-Fitting Basis Sets for H to Rn. *Phys. Chem. Chem. Phys.* **2006**, *8*, 1057−1065. **(b)** Weigend, F.; Ahlrichs, R. Balanced Basis Sets of Split Valence, Triple Zeta Valence and Quadruple Zeta Valence Quality for H to Rn: Design and Assessment of Accuracy. *Phys. Chem. Chem. Phys.* **2005**, *7*, 3297−3305.

(5) **(a)** Neese, F. The ORCA Program System. *Wiley Interdiscip. Rev.: Comput. Mol. Sci.* **2012**, *2*, 73−78. **(b)** Neese, F. Software Update: The ORCA Program System, Version 4.0. *Wiley Interdiscip. Rev.: Comput. Mol. Sci.* **2018**, *8*, No. e1327. **(c)** Neese, F. Software Update: The ORCA Program System–Version 5.0. *Wiley Interdiscip. Rev.: Comput. Mol. Sci.* **2022**, No. e1606.

(6) Grimme, S. Supramolecular Binding Thermodynamics by Dispersion-Corrected Density Functional Theory, *Chem. Eur. J.* **2012,** *18*, 9955−9964.

(7) Gaussian 16, Revision A.03, Frisch, M. J.; Trucks, G. W.; Schlegel, H. B.; Scuseria, G. E.; Robb, M. A.; Cheeseman, J. R.; Scalmani, G.; Barone, V.; Petersson, G. A.; Nakatsuji, H.; Li, X.; Caricato, M.; Marenich, A. V.; Bloino, J.; Janesko, B. G.; Gomperts, R.; Mennucci, B.; Hratchian, H. P.; Ortiz, J. V.; Izmaylov, A. F.; Sonnenberg, J. L.; Williams-Young, D.; Ding, F.; Lipparini, F.; Egidi, F.; Goings, J.; Peng, B.; Petrone, A.; Henderson, T.; Ranasinghe, D.; Zakrzewski, V. G.; Gao, J.; Rega, N.; Zheng, G.; Liang, W.; Hada, M.; Ehara, M.; Toyota, K.; Fukuda, R.; Hasegawa, J.; Ishida, M.; Nakajima, T.; Honda, Y.; Kitao, O.; Nakai, H.; Vreven, T.; Throssell, K.; Montgomery, J. A., Jr.; Peralta, J. E.; Ogliaro, F.; Bearpark, M. J.; Heyd, J. J.; Brothers, E. N.; Kudin, K. N.; Staroverov, V. N.; Keith, T. A.; Kobayashi, R.; Normand, J.; Raghavachari, K.; Rendell, A. P.; Burant, J. C.; Iyengar, S. S.; Tomasi, J.; Cossi, M.; Millam,

J. M.; Klene, M.; Adamo, C.; Cammi, R.; Ochterski, J. W.; Martin, R. L.; Morokuma, K.; Farkas, O.; Foresman, J. B.; Fox, D. J. Gaussian, Inc., Wallingford CT, 2016.

(8) **(a)** Bader, R. F. W. Atoms in Molecules: A Quantum Theory; International Series of Monographs in Chemistry, Vol. 2; Oxford University Press: Oxford, U.K., 1990. **(b)** Popelier, P. Atoms in Molecules: An Introduction; Prentice Hall: Harlow, U.K., 2000. **(c)** The Quantum Theory of Atoms in Molecules: From Solid State to DNA and Drug Design; Matta, C. F., Boyd, R. J., Eds.; Wiley-VCH: Weinheim, Germany, 2007. **(d)** Bader, R. F. W. A Bond Path: A Universal Indicator of Bonded Interactions, *J. Phys. Chem. A* **1998**, *102*, 7314.

(9) Rosenblum, B.; Nethercot, A. H.; Townes, C. H, Isotopic Mass Ratios, Magnetic Moments and the Sign of the Electric Dipole Moment in Carbon Monoxide, *Phys. Rev.* **1958**, *109*, 400–412.

(10) Grimaldi, F.; Lecount, A; Moser, C. The Calculation of the Electric Dipole Moment of CO, *Int. J. Quantum Chem.* **1967**, *1*, 153–161.

(11) **(a)** Riplinger, C.; Neese, F. An Efficient and near Linear Scaling Pair Natural Orbital Based Local Coupled Cluster Method. *J. Chem. Phys.* **2013**, *138*, No. 034106. **(b)** Riplinger, C.; Pinski, P.; Becker, U.; Valeev, E. F.; Neese, F. Sparse Maps - A Systematic Infrastructure for Reduced-Scaling Electronic Structure Methods. II. Linear Scaling Domain Based Pair Natural Orbital Coupled Cluster Theory. *J. Chem. Phys.* **2016**, *144*, No. 024109.

(12) **(a)** Weigend, F. A Fully Direct RI-HF Algorithm: Implementation, Optimised Auxiliary Basis Sets, Demonstration of Accuracy and Efficiency. *Phys. Chem. Chem. Phys.* **2002**, *4*, 4285–4291. **(b)** Hamel, S.; Casida, M. E.; Salahub, D. R. Assessment of the Quality of Orbital Energies in Resolution-of-the-Identity Hartree-Fock Calculations Using DeMon Auxiliary Basis Sets. *J. Chem. Phys.* **2001**, *114*, 7342–7350. **(c)** Früchtl, H. A.; Kendall, R. A.; Harrison, R. J.; Dyall, K. G. An Implementation of RI–SCF on Parallel Computers. *Int. J. Quantum Chem.* **1997**, *64*, 63–69. **(d)** Polly, R.; Werner, H. J.; Manby, F. R.; Knowles, P. J. Fast Hartree-Fock Theory Using Local Density Fitting Approximations. *Mol. Phys.* **2004**, *102*, 2311–2321.

(13) Boys, S. F. Construction of Some Molecular Orbitals to Be Approximately Invariant for Changes from One Molecule to Another. *Rev. Mod. Phys.* **1960**, *32*, 296–299.

(14) **(a)** Dunning, T. H. Gaussian Basis Sets for Use in Correlated Molecular Calculations. I. The Atoms Boron through Neon and Hydrogen. *J. Chem. Phys.* **1989**, *90*, 1007–1023. **(b)** Balabanov, N. B.; Peterson, K. A. Systematically Convergent Basis Sets for Transition Metals. I. All-Electron Correlation Consistent Basis Sets for the 3d Elements Sc–Zn. *J. Chem. Phys.* **2005**, *123*, 064107. **(c)** Peterson, K. A.; Dunning, T. H. Accurate Correlation Consistent Basis Sets for Molecular Core–Valence Correlation Effects: The Second Row Atoms Al–Ar, and the First Row Atoms B–Ne Revisited. *J. Chem. Phys.* **2002**, *117*, 10548–10560.

(15) **(a)** Neese, F.; Hansen, A.; Liakos, D. G. Efficient and Accurate Approximations to the Local Coupled Cluster Singles Doubles Method Using a Truncated Pair Natural Orbital Basis. *J. Chem. Phys.* **2009**, *131*, 064103. **(b) For equivalent simplified forms of the extrapolation formulas and parameters, for example, see SI of the following paper:** Altun, A.; Ghosh, S.; Riplinger, C.; Neese, F.; Bistoni, G. Addressing the System-Size Dependence of the Local Approximation Error in Coupled-Cluster Calculations. *J. Phys. Chem. A* **2021**, *125*, 9932–9939.

(16) Boys, S. F.; Bernardi, F. The Calculation of Small Molecular Interactions by the Differences of Separate Total Energies. Some Procedures with Reduced Errors. *Mol. Phys.* **1970**, *19*, 553–566.

(17) **(a) For closed-shell LED, see:** Schneider, W. B.; Bistoni, G.; Sparta, M.; Saitow, M.; Riplinger, C.; Auer, A. A.; Neese, F. Decomposition of Intermolecular Interaction Energies within the Local Pair Natural Orbital Coupled Cluster Framework. *J. Chem. Theory Comput.* **2016**, *12*, 4778–4792. **(b) For frozen-state LED and DID plots, see:** Altun, A.; Neese, F.;

Bistoni, G. Effect of Electron Correlation on Intermolecular Interactions: A Pair Natural Orbitals Coupled Cluster Based Local Energy Decomposition Study. *J. Chem. Theory Comput.* **2019**, *15*, 215–228. **(c) For open-shell LED, see:** Altun, A.; Saitow, M.; Neese, F.; Bistoni, G. Local Energy Decomposition of Open-Shell Molecular Systems in the Domain-Based Local Pair Natural Orbital Coupled Cluster Framework. *J. Chem. Theory Comput.* **2019**, *15*, 1616–1632. **(d) For a review of LED and related methods, see:** Bistoni, G. Finding Chemical Concepts in the Hilbert Space: Coupled Cluster Analyses of Noncovalent Interactions. *Wiley Interdiscip. Rev. Comput. Mol. Sci.* **2019**, e1442. **(e) For comparision of LED and SAPT terms, see:** Altun, A.; Izsák, R.; Bistoni, G. Local Energy Decomposition of Coupled-cluster Interaction Energies: Interpretation, Benchmarks, and Comparison with Symmetry-adapted Perturbation Theory. *Int. J. Quantum Chem.* **2021**, *121*, e26339.

(18) Lu, Q.; Neese, F.; Bistoni, G. London Dispersion Effects in the Coordination and Activation of Alkanes in σ-Complexes: A Local Energy Decomposition Study. *Phys. Chem. Chem. Phys.* **2019**, *2019*, 11569–11577.

(19) Altun, A.; Neese, F.; Bistoni, G. Open-Shell Variant of the London Dispersion-Corrected Hartree–Fock Method (HFLD) for the Quantification and Analysis of Noncovalent Interaction Energies. *J. Chem. Theory Comput.* **2022**, *18*, 2292–2307.